



<b>Title</b>	What Determines the Shape of a Pine-Island-Like Ice Shelf?
<b>Author(s)</b>	Nakayama, Yoshihiro; Hirata, Toshiki; Goldberg, Daniel; Greene, Chad A.
<b>Citation</b>	Geophysical research letters, 49(22), e2022GL101272 <a href="https://doi.org/10.1029/2022GL101272">https://doi.org/10.1029/2022GL101272</a>
<b>Issue Date</b>	2022-11-14
<b>Doc URL</b>	<a href="http://hdl.handle.net/2115/89234">http://hdl.handle.net/2115/89234</a>
<b>Rights</b>	Copyright 2022 American Geophysical Union.
<b>Type</b>	article
<b>File Information</b>	Geophysical Research Letters - 2022 - Nakayama - What Determines the Shape of a Pine-Island-Like Ice Shelf.pdf



[Instructions for use](#)

# Geophysical Research Letters<sup>®</sup>

## RESEARCH LETTER

10.1029/2022GL101272

### Key Points:

- Ocean melting and ice stretching caused by ice acceleration both thin the ice shelf from the grounding line toward the ice shelf front
- Ice divergence from the center advects ice toward the ice shelf edges, compensating melt-driven thinning
- Ice shelf melting at shallow depths modifies ice shelf shape and contributes to ice shelf front thinning

### Supporting Information:

Supporting Information may be found in the online version of this article.

### Correspondence to:

Y. Nakayama and T. Hirata,  
Yoshihiro.Nakayama@lowtem.hokudai.ac.jp;  
t.hira2112@gmail.com

### Citation:

Nakayama, Y., Hirata, T., Goldberg, D., & Greene, C. A. (2022). What determines the shape of a Pine-Island-like ice shelf? *Geophysical Research Letters*, 49, e2022GL101272. <https://doi.org/10.1029/2022GL101272>

Received 14 SEP 2022

Accepted 9 NOV 2022

### Author Contributions:

**Conceptualization:** Yoshihiro Nakayama, Daniel Goldberg  
**Data curation:** Toshiaki Hirata  
**Formal analysis:** Yoshihiro Nakayama, Toshiaki Hirata  
**Investigation:** Yoshihiro Nakayama, Toshiaki Hirata  
**Methodology:** Yoshihiro Nakayama, Daniel Goldberg  
**Supervision:** Yoshihiro Nakayama  
**Visualization:** Yoshihiro Nakayama  
**Writing – original draft:** Yoshihiro Nakayama, Toshiaki Hirata  
**Writing – review & editing:** Yoshihiro Nakayama, Daniel Goldberg

## What Determines the Shape of a Pine-Island-Like Ice Shelf?

Yoshihiro Nakayama<sup>1</sup> , Toshiaki Hirata<sup>2</sup>, Daniel Goldberg<sup>3</sup> , and Chad A. Greene<sup>4</sup> 

<sup>1</sup>Institute of Low Temperature Science, Hokkaido University, Sapporo, Japan, <sup>2</sup>Graduate School of Environmental Science, Hokkaido University, Sapporo, Japan, <sup>3</sup>School of Geosciences, University of Edinburgh, Edinburgh, UK, <sup>4</sup>Jet Propulsion Laboratory, California Institute of Technology, Pasadena, CA, USA

**Abstract** Ice shelf shape directly controls ocean heat intrusions, melting near the grounding line, and buttressing. Little is known about what determines ice-shelf shape because ice-ocean coupled simulations typically aim at projecting Antarctica's contribution to sea-level rise and they do not resolve small-scale ice-ocean interactive processes. We conduct ice-ocean coupled simulations for an idealized high-resolution, Pine-Island-like model configuration. We show that ocean melting and ice stretching caused by acceleration thin the ice shelf from the grounding line toward the ice shelf front, consistent with previous studies. In the across-flow direction, ocean melting and ice advection cancel each other out and flatten the ice shelf. More than one-third of the ice thinning from grounding line to ice front can be attributed to ocean melting at depths shallower than 500 m. Our results emphasize the importance of interactive processes between the entire ice shelf and the ocean for determining the ice shelf shape.

**Plain Language Summary** Antarctic ice flows into the ocean and forms a floating extension of land ice called an ice shelf. The ice shelf shape directly controls the amount of ocean heat intrusions, melting near the grounding line, and buttressing. However, little is understood about ice-ocean interactive processes determining ice shelf shape because (a) ocean modelers apply a constant cavity geometry, (b) ice modelers mostly assume simplified melting parameterization, and (c) ice-ocean coupled simulations typically aim at projections of Antarctica's sea-level contributions and they require long model integration. We conduct ice-ocean coupled simulations for an idealized high-resolution Pine-Island-like model configuration. Basal melting and ice stretching create a typical ice shelf shape with steep thinning near the grounding line followed by gradual thinning toward the ice shelf front. In the across-flow direction, ice divergence from the center advects ice toward edges, compensating for melt-driven thinning and flattening ice shelf shape. We also show that ice melting at shallow depths contributes to about one-third of ice-shelf thinning. Although it is thought that ice shelf melting at the grounding line dominantly controls ice shelf behavior, our results suggest the importance of ice-ocean interactive processes for the entire ice shelf cavity for determining the ice shelf shape.

## 1. Introduction

West Antarctic ice shelves experienced grounding line retreat, thinning, and acceleration over the past four decades (e.g., Rignot et al. (2019)). Some studies indicate that ice-shelf geometry and its evolution likely substantially impacted ice shelf and glacier evolutions (Jenkins et al., 2010; Smith et al., 2017). For example, (a) steepening of ice-shelf slope likely increases ice-shelf melting near the grounding zones (Jenkins, 1991, 2011, 2016; Lazeroms et al., 2018, 2019), (b) thinning of ice front may reduce barrier effects and may allow stronger warm ocean heat intrusions into ice shelf cavities (Grosfeld et al., 1997; Wählin et al., 2021), and (c) thinning of an ice shelf front can reduce buttressing or remove pinning point critical for ice shelf stability (De Rydt et al., 2014; Joughin et al., 2021; Snow et al., 2017; Wild et al., 2022).

Despite the importance of ice-shelf geometry, we know little about what determines ice shelf shape, because (a) ocean modelers apply a fixed cavity geometry (i.e., Nakayama et al., 2014; St-Laurent et al., 2015; Dinniman et al., 2016; Jourdain et al., 2017; Nakayama et al., 2017, 2019, 2021), (b) ice modelers parameterize ice shelf melt rate using simplified depth-dependent parameterization (e.g., Cornford et al., 2015; Favier et al., 2014; Joughin et al., 2014; Nias et al., 2016) or more sophisticated approaches (e.g., Hill et al., 2021; Lazeroms et al., 2018; McCormack et al., 2021; Pelle et al., 2020; Reese et al., 2018), and (c) ice-ocean coupled simulations typically aim at projecting Antarctica's contribution to sea level and they require long model integration (i.e., Seroussi et al., 2017; Pelle et al., 2021). Remote sensing observations cannot offer much insight into the relations between ice melting and ice stretching because altimetry-based thinning measurements rely on many assumptions leading

to high uncertainty especially close to grounding lines. A few studies have investigated determining factors for ice shelf shape (Little et al., 2012; Sergienko et al., 2013). Sergienko et al. (2013) coupled a 1-D ice flow model (Dupont & Alley, 2005) with the 1-D plume model (Jenkins, 1991) and showed that, over most of the ice shelf, ice thickness advection and ice shelf melting are dominant terms in the ice shelf mass balance equation for a warm ice shelf cavity. However, the width-averaged nature of the study and use of a plume to represent ice-ocean interaction limits their ability to study the impact of spatially changing ocean circulation on ice shelf evolution.

In this study, we use a coupled ice-ocean model, combined with ice shelf-only model configurations and analysis of satellite data, to investigate the ice-shelf processes determining the shape of a Pine-Island-like ice shelf using an idealized configuration (e.g., Asay-Davis et al. (2016), Jordan et al. (2017), and De Rydt and Gudmundsson (2016)). We also perform three coupled sensitivity experiments with varying horizontal resolutions.

## 2. Methods and Experiments

### 2.1. Ice-Ocean Coupled Model

We design our model domain to represent a typical warm-water ice shelf using MITgcm (Losch, 2008; Marshall et al., 1997) as described in Text in Supporting Information S1. The coupled simulation is conducted for 60 years (hereafter CTRL), which reaches a steady state by the end of this period (Jordan et al., 2017). This model is almost identical to Jordan et al. (2017) and the only difference is the north-south extent of the model domain, which is changed from 160 to 100 km. The model domain is 60 km wide, 100 km long, and 1,100 m deep. Nominal horizontal and vertical grid resolutions are 1,000 and 10 m, respectively, for the CTRL case. The ice shelf has an initial extent of 60 km, beyond which it is not allowed to advance. The grounding line is fixed at the boundary and the ice shelf flows into the domain at a constant rate of  $80 \text{ km}^3 \text{ s}^{-1}$  through a boundary we refer to as “south,” and calves in the opposite direction which we refer to as “north” (Figure 1a). Initial temperature and salinity profiles have warm, salty water ( $1.2^\circ\text{C}$ , 34.7) at depth and cold, fresh water at the surface ( $-1^\circ\text{C}$ , 34.0) as shown in Figure S1 in Supporting Information S1. Temperature and salinity are restored to initial conditions at the northern boundary in a five-cell-wide linear sponge layer over a period of 1 day. All boundaries are solid walls and no restoring is applied for ocean velocity and no-slip condition is applied for ice velocity.

### 2.2. Ice Shelf Model

We carry out ice-shelf-only experiments by turning off the ocean model. For the ice-only control case (hereinafter IOCTRL), the ice model is forced by recorded 10-daily mean ice shelf melt rates of CTRL. There is no coupling between the evolving ice geometry and melt rate. The rationale of IOCTRL is to create an experiment which behaves the same as CTRL, but for which we can add or remove ice-dynamical factors without impacting the melt, allowing us to identify leading factors determining the ice shelf shape (Table 1).

### 2.3. Sensitivity Experiments

We also conduct 20-year coupled experiments with varying horizontal grid spacings, which are named 250, 500, and 1000-m cases (see Text in Supporting Information S1 for detail).

## 3. Results

### 3.1. Ice-Ocean Coupled Simulation

The annual mean (year 60) potential temperature section along the centerline (Figure 1a) shows intrusions of warm mCDW toward the ice shelf grounding line. Strong clockwise ocean circulation is located north of the model domain (Figure 1b). High ice-shelf melting of  $\sim 100 \text{ m yr}^{-1}$  is observed along the area close to the grounding line (Figure 1e). These features are similar to Jordan et al. (2017). After 60 years, ice shelf shape converges (as discussed in Jordan et al. (2017)) and steady ice shelf shape shows a steep slope close to the grounding line, and gradual thinning away from the grounding line toward the ice shelf front (Figure 2g) similar to the Pine Island Ice Shelf (e.g., Shean et al. (2018) and Nakayama et al. (2021)).

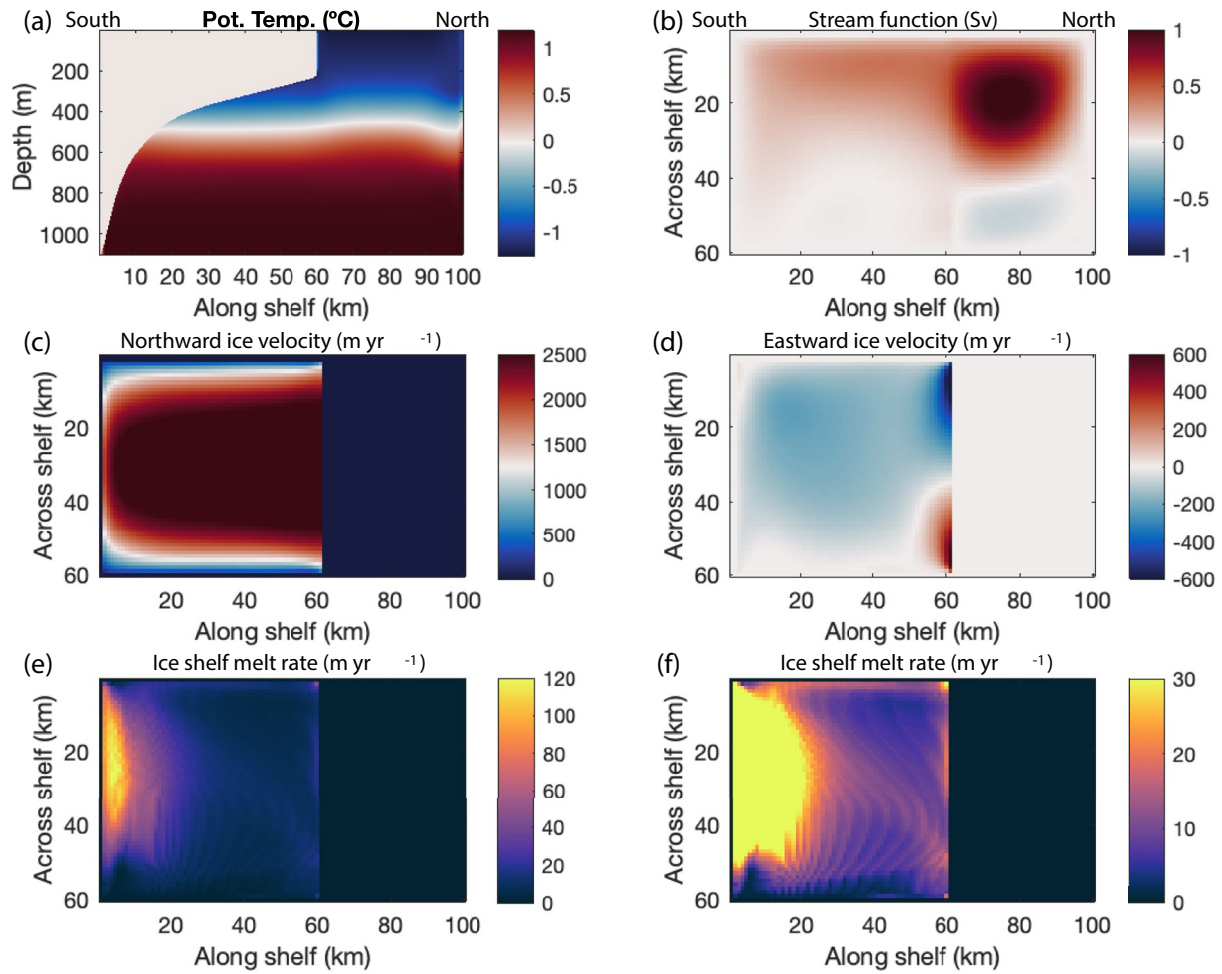


**Figure 1.** (a) Year 60 annual mean vertical section of potential temperature along the centerline for CTRL. (b) Year 60 mean barotropic stream function for CTRL. (c and d) Northward and eastward ice velocities for CTRL. (e and f) Year 60 mean ice shelf melt rate for CTRL using two different color scales. We define the grounding line as the south side and the opposite side as the north as indicated in panels (a and b).

**Table 1**  
*Description of Ice-Only Sensitivity Experiments*

Simulation	Description	Centerline figures	Ice front figures
IOCTRL	Ice only control simulation (identical to M(all)V(dyn)U(dyn))	Figures 2a, 2b, 2d, and 2e	Figures 2c and 2f
M(all)V(dyn)U(0)	Same as IOCTRL but eastward ice velocity fixed to zero	Figures 2a and 2d	Figures 2c and 2f
M(20)V(dyn)U(0)	Same as M(all)V(dyn)U(0) but ice shelf melt rate entirely set to 20 m yr <sup>-1</sup>	Figures 2a and 2d	Figures 2c and 2f
M(all)V(2000)U(0)	Same as M(all)V(dyn)U(0) but northward ice velocity fixed at 2000 m yr <sup>-1</sup>	Figures 2a and 2d	Figures 2c and 2f
M(20)V(2000)U(0)	Same as M(all)V(dyn)U(0) but ice shelf melt rate entirely set to 20 m yr <sup>-1</sup> and northward ice velocity fixed at 2000 m yr <sup>-1</sup>	Figures 2a and 2d	Figures 2c and 2f
M(GL20)V(dyn)U(0)	Same as M(all)V(dyn)U(0) but ice shelf melt only applied within 20 km from the grounding line	Figures 2b and 2e	Figures 2c and 2f
M(GL10)V(dyn)U(0)	Same as M(all)V(dyn)U(0) but ice shelf melt only applied within 10 km from the grounding line	Figures 2b and 2e	Figures 2c and 2f

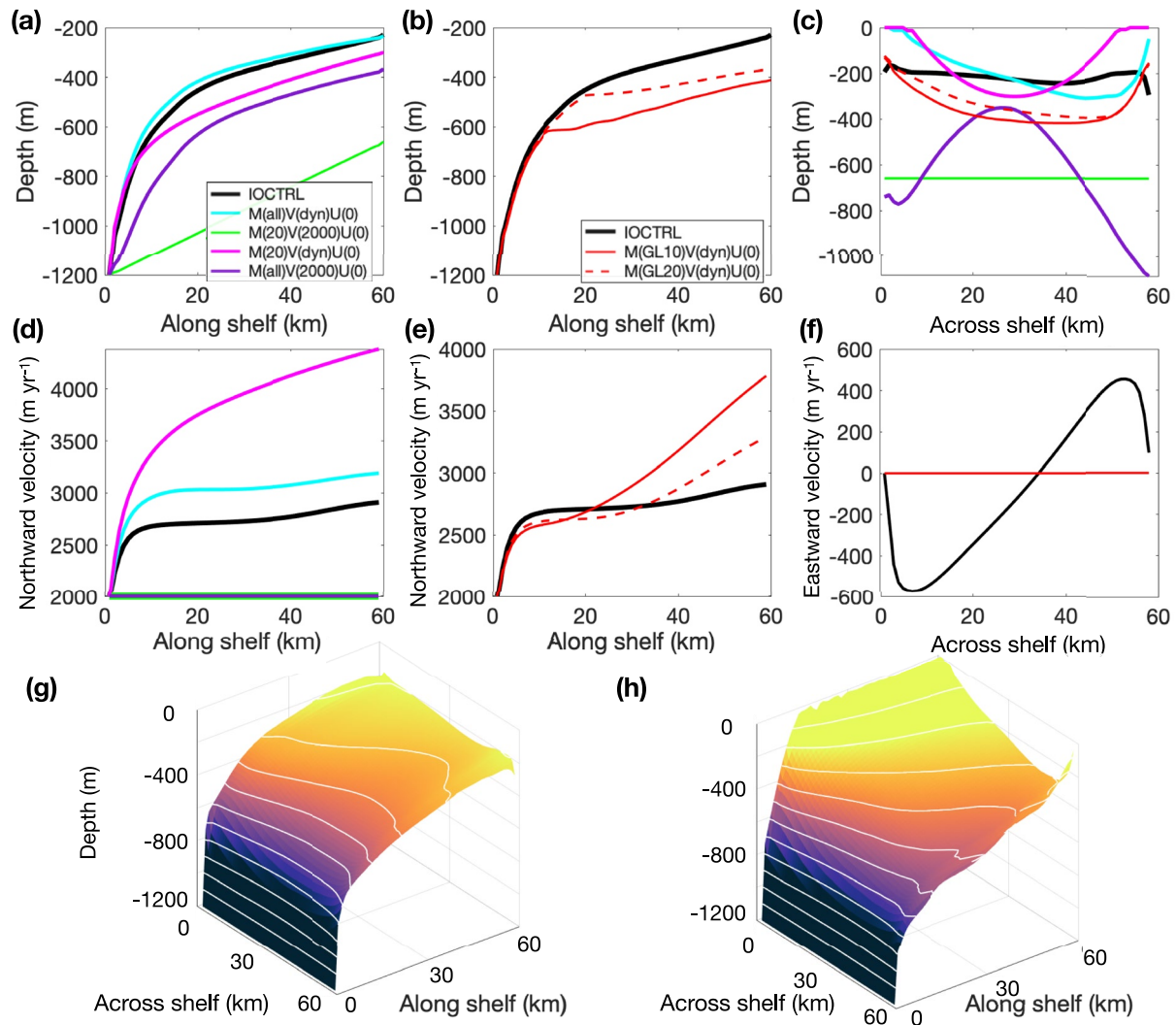


**Figure 2.** Ice shelf cavity shapes along (a and b) the center line and (c) ice shelf front at the end of the model simulation. (d,e) Same as (a and b) but for northward ice velocity, respectively. (f) Same as (c) but for eastward ice velocity. The same color code as (a and b) is applied for other figures. In (f), note that all experiments except for IOCTRL have zero velocity along the across-shelf direction. Ice-shelf shapes (colors, 100 m depth contours) for (g) CTRL and (h) M(all)V(dyn)U(0) at the end of the model simulation.

Northward ice velocity increases from the grounding line toward the ice front (Figure 1c). Within 10 km from the grounding line, ice accelerates from 2000 to 2,700  $\text{m yr}^{-1}$ . Ice velocity stays at  $\sim 2,700 \text{ km}^{-1}$  between 10 and 30 km from the grounding line and it gradually increases to 2,900  $\text{km yr}^{-1}$  close to the ice shelf front (Figure 2g). Similar features can be detected in observations, despite that the observed ice velocity of the Pine Island Ice Shelf is about 1.5 times faster (Joughin et al., 2021). Simulated ice velocity in the across-flow direction presents a divergent feature (Figures 1d and 2f). These asymmetric features are likely formed by accumulated ice shelf melting along the ice shelf edges close to the ice shelf front due to slow northward ice velocity, taking more time for ice to move from the grounding line to the ice front.

### 3.2. Uncoupled Ice Simulation

The steady-state shape of IOCTRL after 60 years matches with the CTRL case with mean differences of  $1.25 \pm 0.4 \text{ m}$  (Figure S2 in Supporting Information S1) for the entire ice shelf. Thus, we use IOCTRL to determine leading factors influencing the ice shelf shape (Table 1).

Ice shelf shapes of IOCTRL and M(all)V(dyn)U(0) are similar with a mean difference of  $\sim 27$  m, suggesting that ice movement in the across-flow direction does not change ice shelf shape along the centerline (Figure 2a). The ice-shelf melting and ice acceleration, however, substantially impact ice shelf shape. The ice shelf shape of the M(all)V(2000)U(0) case (Table 1) shows steep thinning close to the grounding line but the ice shelf slope is about  $\sim 1.3$  times more gentle within 20 km from the grounding line forming a thick ice shelf. The M(20)V(dyn)U(0) case shows an excellent agreement with IOCTRL in terms of ice shelf shape in the first 10 km from the grounding line. Simulated ice velocity, however, shows continuous acceleration from the grounding line to the ice shelf front and ice velocity at the ice shelf front is higher than that of IOCTRL by  $\sim 1.5$  times (Figure 2d), which is different from observations (Joughin et al., 2021). For the M(20)V(2000)U(0) case, the ice shelf bottom has a constant slope, which implies that ice shelf melting and ice acceleration form steep ice slopes close to the grounding line. We note that ice shelf melt rate and ice velocity of 20 and 2,000  $\text{m yr}^{-1}$ , respectively, are spatial averages.

We also investigate the importance of ice-shelf melting close to the grounding line (Table 1). Close to the grounding line, the ice shelf shapes simulated in the M(GL20)V(dyn)U(0) and M(GL10)V(dyn)U(0) cases show good agreement with the IOCTRL. Away from the grounding line, ice shelf thickness remains thick for both two cases with simulated thicknesses of  $\sim 400$  m and  $\sim 380$  m for M(GL20)V(dyn)U(0) and M(GL10)V(dyn)U(0) cases, respectively (Figure 2b). When ice shelf melt is turned off, ice velocity starts to increase toward the ice shelf front reaching 3,300 and 3,800  $\text{m yr}^{-1}$ , respectively, for the M(GL20)V(dyn)U(0) and M(GL10)V(dyn)U(0) cases (Figure 2e).

At the ice shelf front, the IOCTRL shapes are relatively flat with a slight deepening eastward from  $\sim 180$  to  $\sim 200$  m, while most ice shelf shapes with U(0) become thinner at both east and west sides (Figure 2c) by about  $\sim 200$  m compared to IOCTRL. The ice shelf shape becomes transversely flat for the M(20)V(2000)U(0) case and the ice shelf becomes thinner in the middle for the M(all)V(2000)U(0) case (Figure 2c). These differences can be explained primarily by ice velocity. When northward ice movement is slow, especially at the eastern and western ice shelf edges, it takes a long time for ice to reach the ice shelf front allowing the ocean to melt and thin the ice shelf. When ice velocity is set to constant (e.g., M(all)V(2000)U(0)), ice shelf front thickness becomes thinner in the middle reflecting the spatial pattern of ice-shelf melting (Figures 1e and 1f).

In summary, ice shelf shapes with steep and gradual thinning close to and away from the grounding line, respectively, are formed by ice acceleration and ice-shelf melting with a peak close to the grounding line. The relatively flat ice-shelf shape along the cross-flow direction is created as a balance between ice shelf melting and ice advection (Figure 2c).

### 3.3. Coupled Sensitivity Experiments

Ice shelf shapes are qualitatively similar for the 250, 500, and 1000-m cases (Figure S3 in Supporting Information S1). High resolution allows the ice shelf to form a steeper slope close to the grounding line, which enhances the ice shelf melt rate close to the grounding line (Figures S3 and S4 in Supporting Information S1). Peak ice shelf melt rates within 5 km from the grounding line are 93, 86, and 72  $\text{m yr}^{-1}$  for the 250, 500, and 1000-m cases, respectively. Despite some other differences (see Text in Supporting Information S1 for detail), the impact of horizontal resolution on ice shelf shape is smaller than that of other sensitivity experiments (Figure 2).

## 4. Discussion

### 4.1. What Determines the Shape of the Idealized Pine-Island-Like Ice Shelf?

Based on the steady state of the 1-D ice shelf mass balance equation (Equation 14 in Sergienko et al. (2013)), ice thickness change in the along-flow direction can be caused by thinning driven by ice acceleration and ice shelf melting. The derivative of ice thickness with respect to distance from grounding line  $H_y$  can be represented by

$$H_y = -\frac{1}{v} (M + v_y H), \quad (1)$$

where  $y$ ,  $v$ ,  $M$ ,  $H$  are distance from grounding line, northward ice velocity, ice shelf melt rate, and ice thickness, respectively. Using CTRL, we integrate  $-M/v$  and  $-v_y H/v$  from the grounding line to the ice shelf front to calculate cumulative ice shelf thickness changes by ice shelf melting and ice acceleration along the centerline,

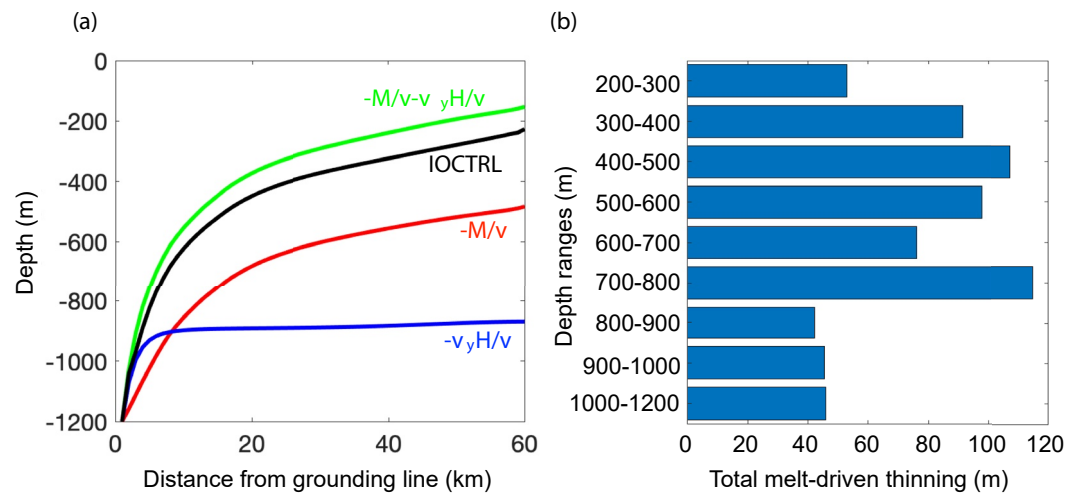


**Figure 3.** (a) Simulated CTRL ice shelf shape (black) and ice shelf shapes calculated considering ice-dynamics-driven thinning (blue) and melt-driven thinning (red). The ice shelf shape considering both ice-dynamics-driven thinning and melt-driven thinning is shown in green. (b) Bar diagram showing relations between ice shelf depth and total thinning due to ice shelf melting for CTRL.

respectively. The ice shelf shape obtained by summing these two effects together is similar to CTRL with the difference in ice shelf thickness of about 70 m at the ice shelf front (Figure 3a). This suggests that the 1D (along flow) mass balance equation can roughly explain ice shelf shape, neglecting transverse divergence and advection. The ice acceleration term steeply decreases ice thickness within 2–3 km from the grounding line. At 1, 3, and 5 km from the grounding line, ice shelf thinning due to ice acceleration (ice shelf melting) is 70 (42), 245 (134), and 283 m (217 m), respectively (Figure 3a and Figure S5 in Supporting Information S1). Beyond 10 km away from the grounding line, ice acceleration does not contribute greatly to ice shelf thinning and the ice shelf continues to thin as a result of ice-shelf melting, as suggested by Sergienko et al. (2013). In total, ice acceleration and ice shelf melting contribute to 331 and 716 m of along-flow ice-shelf thinning, respectively. About 37% of ice shelf melting along the centerline occurs at depths deeper than 700 m (Figure 3b).

Our aims are to identify processes determining ice shelf shape in the along-flow direction with steep and gentle thinning close to and away from the grounding line, respectively. Thus, we utilize a simple case presented in Jordan et al. (2017). Ice boundary conditions (no-slip or partial slip) and ice flux at the grounding line likely modulate ice shelf shape as well, but sensitivity experiments for these parameters remain for future work.

#### 4.2. Processes Determining Ice Thickness at Ice Shelf Front

In uncoupled ice simulations, experiments forced by ice shelf melting only within 10 or 20 km from the grounding line (M(GL20)V(dyn)U(0) and M(GL10)V(dyn)U(0)) thicken the ice shelf front by  $\sim 150$  m and  $\sim 190$  m, respectively. In the coupled simulation (CTRL), shallow depth (100–500 m) ice shelf melting contributes to ice shelf thinning by  $\sim 250$  m (Figure 3b). These two results suggest that ice shelf melting at shallow depths can substantially impact ice shelf thickness at the front for warm ice shelf cavities. Such shallow depth melting is not driven by surface water entering the ice shelf cavities (e.g., Jacobs et al. (1992) and Hattermann et al. (2012)) but likely driven by outflowing relatively cold water. Shallow depth melting becomes non-negligible because the ice shelf has a broad area with shallow ice thickness.

#### 4.3. Application to Real Pine Island Ice Shelf

Using observations of Pine Island Ice Shelf (Adusumilli et al., 2020; Gardner et al., 2019; Morlighem et al., 2020), we calculate cumulative ice shelf thickness changes by ice shelf melting and ice acceleration for Pine Island Ice Shelf (Figure 4). We assume that  $v$  and  $v_y$  increase at the rate of doubling every 40 years (Mouginot et al., 2014) (See Text in Supporting Information S1 for detail).

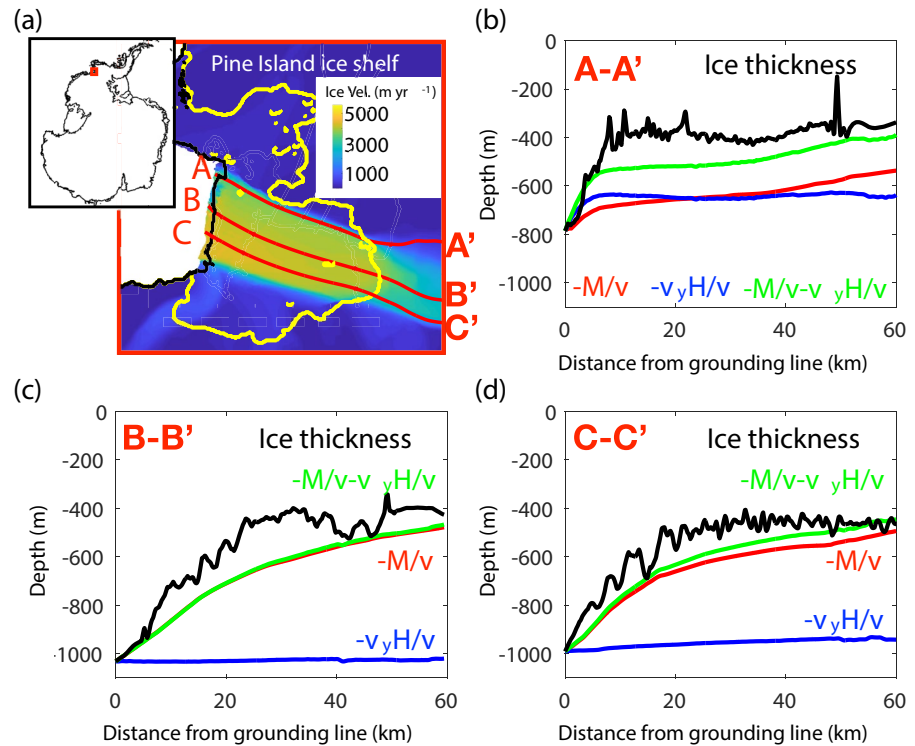


**Figure 4.** (a) Pine Island ice velocity observations from ITS\_LIVE (Gardner et al., 2019). The coastline and grounding lines are shown in black and yellow, respectively. The inset (top left) shows Antarctica with a red box denoting the location of the enlarged portion. (b) Pine Island ice shelf cavity shape (Moriglighem et al., 2020) along the flow line A-A'. Calculated Ice shelf shapes considering ice-dynamics-driven thinning (red) and melt-driven thinning (red) terms based on observed ice velocity (Gardner et al., 2019) and ice shelf melt rate (Adusumilli et al., 2020), respectively, are shown. The estimated ice shelf shape considering both ice-dynamics-driven thinning and melt-driven thinning is shown in green. (c, d) Same as (b) but for B-B' and C-C', respectively. All panels are created using Antarctic mapping tool for MATLAB (Greene et al., 2017).

For A-A', both ice shelf melting and ice acceleration contribute to ice shelf thickness reduction from the grounding line to the ice shelf front. Ice acceleration only contributes to ice shelf thickness reduction within 5 km from the grounding line, presenting qualitatively similar results with simulations. The cumulative ice shelf thickness changes both by ice shelf melting and ice acceleration generally agrees with observed ice thickness with maximum difference of ~150 m (Figure 4b). For B-B' and C-C', ice shelf melting dominantly contributes to ice shelf thickness reduction from the grounding line to the ice shelf front (Figure 4b). Unlike our simulations, ice acceleration does not contribute to ice shelf thickness change. The estimated ice thicknesses assuming the 1-D ice thickness equation (cumulative ice shelf thickness changes both by ice shelf melting and ice acceleration) along B-B' and C-C' generally agree with observations (green and black lines in Figures 4c and 4d). The differences are about 100 and 200 m about 10–20 km downstream from the grounding line for B-B' and C-C', respectively. Such differences are likely caused by the assumption of spatially constant ice shelf melting, no grounding line movement, and 1-D ice flow.

For A-A', ice shelf thickness decreases from 500 to 340 m from 6.2 km away from the grounding line to the ice shelf front. For B-B', ice shelf thickness decreases from 500 to 426 m from 22.5 km away from the grounding line to the ice shelf front. Observed ice shelf thickness along C-C' thins slightly for the region away from the grounding line but showing an even deepening trend from 30 km away from the grounding line to the ice shelf front. These thickness variations along these flow lines indicate that ice shelf melting occurs at shallow depths thinning the ice shelf by 50–150 m along A-A' and B-B' but no obvious shallow depth thinning occurs along C-C'.

Based on observational data, we confirm that ocean melting and ice acceleration are the two main terms shaping the ice shelf. We also show the importance of shallow depth ice shelf melting for modulating ice front thickness for cases A-A' and B-B'.



## 5. Conclusions

We show that ocean melting and ice stretching caused by ice acceleration both thin the ice shelf from the grounding line toward the ice shelf front, while ice divergence from the center advects ice toward the ice shelf edges, compensating melt-driven thinning along the across-shelf direction. We separate the ice dynamical component of ice shelf thinning from melt-induced thinning, as a way to understand processes that occur around the grounding zone, where satellite measurements cannot provide a direct measure of basal melt. In the case of idealized Pine-Island-like ice shelf, ~75% and ~25% of ice-shelf thinning is driven by ice shelf melting and ice stretching, respectively. Melt rates are highest near the deep grounding line, but the ice shelf melting at shallower depths, where most of the ice shelf base sits, modulates ice shelf shapes. Shallow depth (100–500 m) ice shelf melting thins the ice shelf by ~250 m. Recent studies (e.g., Joughin et al., 2021; Wählin et al., 2021) show that ice shelf shape close to the ice shelf front can control ice shelf buttressing, ice shelf/glacier evolutions, and sea level rise prediction. This study suggests that ice-ocean interactive processes between the entire ice shelf and the ocean alter ice shelf shape including ice shelf front thickness, despite that ice-ocean interactive processes only close to grounding zones have attracted much attention in the past decades.

## Data Availability Statement

The model code, input, and results are available at <https://zenodo.org/record/6451059#.Y28oYOxBxRF>. The model code and input files can also be found at [https://github.com/hgu784/MITgcm\\_67s](https://github.com/hgu784/MITgcm_67s).

## References

- Adusumilli, S., Fricker, H. A., Medley, B., Padman, L., & Siegfried, M. R. (2020). Interannual variations in meltwater input to the Southern Ocean from Antarctic ice shelves. *Nature Geoscience*, 13(9), 616–620. <https://doi.org/10.1038/s41561-020-0616-z>
- Asay-Davis, X. S., Cornford, S. L., Durand, G., Galton-Fenzi, B. K., Gladstone, R. M., Gudmundsson, G. H., et al. (2016). Experimental design for three interrelated marine ice sheet and ocean model intercomparison projects: Mismip v. 3 (mismip+), isomip v. 2 (isomip+) and mismip v. 1 (mismip1). *Geoscientific Model Development*, 9(7), 2471–2497. <https://doi.org/10.5194/gmd-9-2471-2016>
- Cornford, S. L., Martin, D. F., Payne, A. J., Ng, E. G., Le Brocq, A. M., Gladstone, R. M., et al. (2015). Century-scale simulations of the response of the West Antarctic Ice Sheet to a warming climate. *The Cryosphere*, 9(4), 1579–1600. <https://doi.org/10.5194/tc-9-1579-2015>
- De Rydt, J., & Gudmundsson, G. (2016). Coupled ice shelf-ocean modeling and complex grounding line retreat from a seabed ridge. *Journal of Geophysical Research*, 121(5), 865–880. <https://doi.org/10.1002/2015JF003791>
- De Rydt, J., Holland, P., Dutrieux, P., & Jenkins, A. (2014). Geometric and oceanographic controls on melting beneath pine Island glacier. *Journal of Geophysical Research: Oceans*, 119(4), 2420–2438. <https://doi.org/10.1002/2013jc009513>
- Dinniman, M. S., Asay-Davis, X. S., Galton-Fenzi, B. K., Holland, P. R., Jenkins, A., & Timmermann, R. (2016). Modeling ice shelf/ocean interaction in Antarctica: A review. *Oceanography*, 29(4), 144–153. <https://doi.org/10.5670/oceanog.2016.106>
- Dupont, T. K., & Alley, R. B. (2005). Assessment of the importance of ice-shelf buttressing to ice-sheet flow. *Geophysical Research Letters*, 32(4), L04503. <https://doi.org/10.1029/2004gl020204>
- Favier, L., Durand, G., Cornford, S. L., Gudmundsson, G. H., Gagliardini, O., Gillet-Chaulet, F., et al. (2014). Retreat of Pine Island Glacier controlled by marine ice-sheet instability. *Nature Climate Change*, 4(2), 117–121. <https://doi.org/10.1038/NCLIMATE2094>
- Gardner, A. S., Fahnestock, M., & Scambos, T. A. (2019). *ITS\_LIVE regional glacier and ice sheet surface velocities*. Data archived at national snow and ice data center. <https://doi.org/10.5067/6116VW8LLWJ7>
- Greene, C. A., Gwyther, D. E., & Blankenship, D. D. (2017). Antarctic mapping tools for MATLAB. *Computers & Geosciences*, 104, 151–157. <https://doi.org/10.1016/j.cageo.2016.08.003>
- Grosfeld, K., Gerdes, R., & Determann, J. (1997). Thermohaline circulation and interaction between ice shelf cavities and the adjacent open ocean. *Journal of Geophysical Research*, 102(C7), 15595–15610. <https://doi.org/10.1029/97jc00891>
- Hattermann, T., Nøst, O. A., Lilly, J. M., & Smedsrud, L. H. (2012). Two years of oceanic observations below the fimbul ice shelf, Antarctica. *Geophysical Research Letters*, 39(12). <https://doi.org/10.1029/2012gl051012>
- Hill, E. A., Rosier, S. H., Gudmundsson, G. H., & Collins, M. (2021). Quantifying the potential future contribution to global mean sea level from the Filchner–Ronne basin, Antarctica. *The Cryosphere*, 15(10), 4675–4702. <https://doi.org/10.5194/tc-15-4675-2021>
- Jacobs, S., Hellmer, H., Doake, C., Jenkins, A., & Frolich, R. (1992). Melting of ice shelves and the mass balance of Antarctica. *Journal of Glaciology*, 38(130), 375–387. <https://doi.org/10.1017/s0022143000002252>
- Jenkins, A. (1991). A one-dimensional model of ice shelf-ocean interaction. *Journal of Geophysical Research*, 96(C11), 20671–20677. <https://doi.org/10.1029/91jc01842>
- Jenkins, A. (2011). Convection-driven melting near the grounding lines of ice shelves and tidewater glaciers. *Journal of Physical Oceanography*, 41(12), 2279–2294. <https://doi.org/10.1175/jpo-d-11-03.1>
- Jenkins, A. (2016). A simple model of the ice shelf–ocean boundary layer and current. *Journal of Physical Oceanography*, 46(6), 1785–1803. <https://doi.org/10.1175/jpo-d-15-0194.1>
- Jenkins, A., Dutrieux, P., Jacobs, S. S., McPhail, S. D., Perrett, J. R., Webb, A. T., & White, D. (2010). Observations beneath pine Island glacier in west Antarctica and implications for its retreat. *Nature Geoscience*, 3(7), 468–472. <https://doi.org/10.1038/ngeo890>
- Jordan, J. R., Holland, P. R., Goldberg, D., Snow, K., Arthern, R., Heimbach, P., et al. (2017). Ocean-forced ice-shelf thinning in asynchronously coupled ice-ocean model. *Journal of Geophysical Research: Oceans*, 123(2), 864–882. <https://doi.org/10.1002/2017jc013251>
- Joughin, I., Shapero, D., Smith, B., Dutrieux, P., & Barham, M. (2021). Ice-shelf retreat drives recent Pine Island Glacier speedup. *Science Advances*, 7(24), eabg3080. <https://doi.org/10.1126/sciadv.abg3080>

## Acknowledgments

This work was supported by Grants-in-Aids for Scientific Research (21K13989) from the Ministry of Education, Culture, Sports, Science, and Technology in Japan, and NSF ITGC Grant PROPHET. This study is supported by the Cooperative Research Activities of Collaborative Use of Computing Facility of the Atmosphere and Ocean Research Institute, the University of Tokyo. The authors thank Dimitris Menemenlis, Helene Seroussi, and Ayako Abe-Ouchi for their useful comments and suggestions. Insightful comments from the two anonymous reviewers were very helpful for improvement of the manuscript.

- Joughin, I., Smith, B. E., & Medley, B. (2014). Marine ice sheet collapse potentially under way for the thwaites glacier basin, West Antarctica. *Science*, *344*(6185), 735–738. <https://doi.org/10.1126/science.1249055>
- Jourdain, N. C., Mathiot, P., Merino, N., Durand, G., Le Sommer, J., Spence, P., et al. (2017). Ocean circulation and sea-ice thinning induced by melting ice shelves in the Amundsen Sea. *Journal of Geophysical Research: Oceans*, *122*(3), 2550–2573. <https://doi.org/10.1002/2016jc012509>
- Lazeroms, W. M., Jenkins, A., Gudmundsson, G. H., & Van De Wal, R. S. (2018). Modelling present-day basal melt rates for Antarctic ice shelves using a parametrization of buoyant meltwater plumes. *The Cryosphere*, *12*(1), 49–70. <https://doi.org/10.5194/tc-12-49-2018>
- Lazeroms, W. M., Jenkins, A., Rienstra, S. W., & Van De Wal, R. S. (2019). An analytical derivation of ice-shelf basal melt based on the dynamics of meltwater plumes. *Journal of Physical Oceanography*, *49*(4), 917–939. <https://doi.org/10.1175/jpo-d-18-0131.1>
- Little, C. M., Goldberg, D., Gnanadesikan, A., & Oppenheimer, M. (2012). On the coupled response to ice-shelf basal melting. *Journal of Glaciology*, *58*(208), 203–215. <https://doi.org/10.3189/2012jog11j037>
- Losch, M. (2008). Modeling ice shelf cavities in a z coordinate ocean general circulation model. *Journal of Geophysical Research*, *113*(C8), C08043. <https://doi.org/10.1029/2007jc004368>
- Marshall, J., Adcroft, A., Hill, C., Perelman, L., & Heisey, C. (1997). A finite-volume, incompressible Navier Stokes model for studies of the ocean on parallel computers. *Journal of Geophysical Research*, *102*(C3), 5753–5766. <https://doi.org/10.1029/96jc02775>
- McCormack, F., Roberts, J., Gwyther, D., Morlighem, M., Pelle, T., & Galton-Fenzi, B. (2021). The impact of variable ocean temperatures on Totten Glacier stability and discharge. *Geophysical Research Letters*, *48*(10), e2020GL091790. <https://doi.org/10.1029/2020gl091790>
- Morlighem, M., Rignot, E., Binder, T., Blankenship, D., Drews, R., Eagles, G., et al. (2020). Deep glacial troughs and stabilizing ridges unveiled beneath the margins of the Antarctic ice sheet. *Nature Geoscience*, *13*(2), 132–137. <https://doi.org/10.1038/s41561-019-0510-8>
- Mouginot, J., Rignot, E., & Scheuchl, B. (2014). Sustained increase in ice discharge from the Amundsen sea embayment, west Antarctica, from 1973 to 2013. *Geophysical Research Letters*, *41*(5), 1576–1584. <https://doi.org/10.1002/2013GL059069>
- Nakayama, Y., Cai, C., & Seroussi, H. (2021). Impact of subglacial freshwater discharge on pine Island ice shelf. *Geophysical Research Letters*, *48*(18), e2021GL093923. <https://doi.org/10.1029/2021gl093923>
- Nakayama, Y., Manucharayan, G., Kelin, P., Torres, H. G., Schodlok, M., Rignot, E., et al. (2019). Pathway of circumpolar deep water into pine Island and thwaites ice shelf cavities and to their grounding lines. *Scientific Reports*.
- Nakayama, Y., Menemenlis, D., Schodlok, M., & Rignot, E. (2017). Amundsen and Bellingshausen Seas simulation with optimized ocean, sea ice, and thermodynamic ice shelf model parameters. *Journal of Geophysical Research: Oceans*, *122*(8), 6180–6195. <https://doi.org/10.1002/2016jc012538>
- Nakayama, Y., Timmermann, R., Rodehacke, C. B., Schröder, M., & Hellmer, H. H. (2014). Modeling the spreading of glacial meltwater from the Amundsen and bellingshausen seas. *Geophysical Research Letters*, *41*(22), 7942–7949. <https://doi.org/10.1002/2014gl061600>
- Nias, I. J., Cornford, S. L., & Payne, A. J. (2016). Contrasting the modelled sensitivity of the Amundsen Sea Embayment ice streams. *Journal of Glaciology*, *62*(233), 552–562. <https://doi.org/10.1017/jog.2016.40>
- Pelle, T., Morlighem, M., & McCormack, F. S. (2020). Aurora basin, the weak underbelly of East Antarctica. *Geophysical Research Letters*, *47*(9), e2019GL086821. <https://doi.org/10.1029/2019gl086821>
- Pelle, T., Morlighem, M., Nakayama, Y., & Serrousi, H. (2021). Widespread grounding line retreat of Totten Glacier over the 21st century. *Geophysical Research Letters*, *48*(17). <https://doi.org/10.1029/2021gl093213>
- Reese, R., Gudmundsson, G. H., Levermann, A., & Winkelmann, R. (2018). The far reach of ice-shelf thinning in Antarctica. *Nature Climate Change*, *8*(1), 53–57. <https://doi.org/10.1038/s41558-017-0020-x>
- Rignot, E., Mouginot, J., Scheuchl, B., van den Broeke, M., van Wessem, M. J., & Morlighem, M. (2019). Four decades of Antarctic ice sheet mass balance from 1979–2017. *Proceedings of the National Academy of Sciences*, *116*(4), 1095–1103. <https://doi.org/10.1073/pnas.1812883116>
- Sergienko, O., Goldberg, D., & Little, M. C. (2013). Alternative ice shelf equilibria determined by ocean environment. *Journal of Geophysical Research: Earth Surface*, *118*(2), 970–981. <https://doi.org/10.1002/jgrf.20054>
- Seroussi, H., Nakayama, Y., Larour, E., Menemenlis, D., Morlighem, M., Rignot, E., & Khazendar, A. (2017). Continued retreat of Thwaites Glacier, West Antarctica, controlled by bed topography and ocean circulation. *Geophysical Research Letters*, *44*(12), 6191–6199. <https://doi.org/10.1002/2017GL072910>
- Shean, D. E., Joughin, I. R., Dutrieux, P., Smith, B. E., & Berthier, E. (2018). Ice shelf basal melt rates from a high-resolution DEM record for Pine Island Glacier, Antarctica. In *The cryosphere discussions (October)* (pp. 1–39). <https://doi.org/10.5194/tc-2018-209>
- Smith, J. A., Andersen, T., Shortt, M., Gaffney, A., Truffer, M., Stanton, T. P., et al. (2017). Sub-ice-shelf sediments record history of twentieth-century retreat of Pine Island Glacier. *Nature*, *541*(7635), 77–80. <https://doi.org/10.1038/nature20136>
- Snow, K., Goldberg, D., Holland, P. R., Jordan, J. R., Arthern, R. J., & Jenkins, A. (2017). The response of ice sheets to climate variability. *Geophysical Research Letters*, *44*(23), 11–878. <https://doi.org/10.1002/2017gl075745>
- St-Laurent, P., Klinck, J., & Dinniman, M. (2015). Impact of local winter cooling on the melt of Pine Island Glacier, Antarctica. *Journal of Geophysical Research: Oceans*, *120*(10), 6718–6732. <https://doi.org/10.1002/2015jc010709>
- Wählin, A. K., Graham, A. G. C., Hogan, K. A., Queste, B. Y., Boehme, L., Larter, R. D., et al. (2021). Pathways and modification of warm water flowing beneath thwaites ice shelf, west Antarctica. *Science Advances*, *7*(15). <https://doi.org/10.1126/sciadv.abd7254>
- Wild, C. T., Alley, K. E., Muto, A., Truffer, M., Scambos, T. A., & Pettit, E. C. (2022). Weakening of the pinning point buttressing thwaites glacier, west Antarctica. *The Cryosphere*, *16*(2), 397–417. <https://doi.org/10.5194/tc-16-397-2022>

## References From the Supporting Information

- Campin, J.-M., Adcroft, A., Hill, C., & Marshall, J. (2004). Conservation of properties in a free-surface model. *Ocean Modelling*, *6*(3–4), 221–244. [https://doi.org/10.1016/s1463-5003\(03\)00009-x](https://doi.org/10.1016/s1463-5003(03)00009-x)
- Goldberg, D., & Heimbach, P. (2013). Parameter and state estimation with a time-dependent adjoint marine ice sheet model. *The Cryosphere*, *7*(6), 1659–1678. <https://doi.org/10.5194/tc-7-1659-2013>
- Greene, C. A. (2022). Ice flowlines. MATLAB central file exchange.
- Hellmer, H., & Olbers, D. (1989). A two-dimensional model for the thermohaline circulation under an ice shelf. *Antarctic Science*, *1*(04), 325–336. <https://doi.org/10.1017/s0954102089000490>
- Jenkins, A. (1999). The impact of melting ice on ocean waters. *Journal of Physical Oceanography*, *29*(9), 2370–2381. [https://doi.org/10.1175/1520-0485\(1999\)029<2370:tiomio>2.0.co;2](https://doi.org/10.1175/1520-0485(1999)029<2370:tiomio>2.0.co;2)
- Shean, D. E., Christianson, K., Larson, K. M., Ligtenberg, S. R., Joughin, I. R., Smith, B. E., et al. (2017). GPS-derived estimates of surface mass balance and ocean-induced basal melt for Pine Island Glacier ice shelf, Antarctica. *The Cryosphere*, *11*(6), 2655–2674. <https://doi.org/10.5194/tc-11-2655-2017>